Catena 271 (2026) 110242

Contents lists available at ScienceDirect

Catena

journal homepage: www.elsevier.com/locate/catena

Geomorphic flood index 2.0: enhanced tools for delineating flood-prone areas in data-scarce regions

Salvatore Manfreda [a,*], Jorge Saavedra Navarro [a], Cinzia Albertini [a], Ruodan Zhuang [a], Felice Daniele Pacia [a,b], Sadashiv Chaturvedi [a,b], Caterina Samela [c]

[a] Department of Civil, Construction and Environmental Engineering (DICEA), University of Naples Federico II, Naples, Italy
[b] IUSS University School for Advanced Studies of Pavia, Pavia, Italy
[c] National Research Council of Italy - Institute of Methodologies for Environmental Analysis, (CNR-IMAA), Tito Scalo (PZ), Italy

ARTICLE INFO

Keywords:
Flood-prone area mapping
DEM-based flood mapping
Geomorphic flood index
Backwater effects
River confluences
Data-scarce regions

ABSTRACT

Accurately delineating flood-prone areas over large regions remains challenging in areas with limited data, where detailed hydraulic modelling is often impractical. The Geomorphic Flood Index (GFI) is a parsimonious, DEM-based alternative; however, its original formulation may misrepresent inundation near river confluences, where backwater effects and tributary–main stem interactions alter local water levels. This study presents GFI 2.0, an enhanced GFI framework that introduces an iterative confluence module guided by stream hierarchy. This new module accounts for confluence-controlled backwater effects while preserving the original method's simplicity and low computational cost. GFI 2.0 was evaluated across 12 Italian basins using official ISPRA flood hazard maps and multiple DEM products. Additionally, GFI 2.0 was tested with a detailed hydraulic benchmark in the Bradano River basin based on two-dimensional simulations for 30-, 200-, and 500-year return periods. The results show systematic improvements in flood extent delineation, particularly in low-gradient floodplains, wide valleys, and confluence-dominated sectors. Gains are smaller in strongly confined, mountainous basins. A multi-basin analysis indicates that GFI 2.0's added value is greatest when coarser DEMs are used. In the Bradano basin, the area under the curve (AUC) increased from 0.917 to 0.952, from 0.918 to 0.960, and from 0.914 to 0.959 for the 30-, 200-, and 500-year scenarios, respectively. Flood depth estimates improved as well, particularly for larger return periods. RMSE decreased from 5.25 to 3.24 m for the 200-year scenario and from 5.66 to 3.58 m for the 500-year scenario. Overall, GFI 2.0 expands the use of DEM-based flood mapping by offering a scalable, physically informed, and computationally efficient tool for regional screening and preliminary hazard assessment in areas with limited data.

1. Introduction

Reliable flood hazard information is essential for risk management, spatial planning, and emergency response. However, creating and regularly updating flood maps over large areas remains challenging, particularly in regions with limited data. Flood patterns are strongly influenced by the configuration of the river network and the associated catchment geomorphology. These factors govern connectivity, storage, and flood wave propagation (Sofia and Nikolopoulos, 2020; Guse et al., 2020; Yan et al., 2024). Beyond these intrinsic physical controls, external drivers such as climate change, land use changes, urbanisation, and hydraulic infrastructure alter the magnitude and spatial footprint of inundation. This reinforces the need for scalable mapping approaches that support decision-making across multiple spatial scales (Winsemius et al., 2016; Blöschl, 2022; Mishra et al., 2022).

State-of-the-art two-dimensional (2D) hydraulic models can reproduce inundation dynamics and provide depth and velocity fields using fine numerical meshes (De Almeida and Bates, 2013; Hunter et al., 2007; Cea and Costabile, 2022; Perrini et al., 2025). However, these models are data- and resource-intensive and difficult to deploy consistently across large domains. This has stimulated the development of low-complexity methods that exploit topographic information to rapidly delineate flood-prone areas. DEM-based geomorphic and hydro-geomorphic approaches are cost-effective, first-order descriptions of flood susceptibility. These approaches extract the "geomorphic signature" of inundation from terrain structure (Manfreda et al., 2011;

* Corresponding author.
E-mail address: salvatore.manfreda@unina.it (S. Manfreda).

https://doi.org/10.1016/j.catena.2026.110242
Received 15 September 2025; Received in revised form 16 March 2026; Accepted 13 May 2026

Degiorgis et al., 2012; Nardi et al., 2013). Examples include relative-elevation descriptors, such as Height Above the Nearest Drainage (HAND) (Nobre et al., 2016), and geomorphic classifiers, such as the Geomorphic Flood Index (GFI) (Manfreda et al., 2015; Samela et al., 2017a). These indices have been progressively refined to better handle low-relief settings and coastal outlets (Albertini et al., 2022; Arcorace et al., 2024; Aristizabal et al., 2023).

Recent developments indicate a clear convergence towards integrated workflows that combine complementary information sources and modelling philosophies. Three lines of advancement are particularly relevant: (i) the proliferation of consistent, large-area geomorphic floodplain products derived from global digital elevation models (DEMs), such as GFPLAIN250m and SHIFT, which provide baseline envelopes for regional-to-global screening and intercomparison (Nardi et al., 2019; Zheng et al., 2024); (ii) hybrid frameworks that couple geomorphic envelopes with simplified hydrologic-hydraulic modelling and intensity-duration-frequency (IDF) information to generate scenario-based extents and first-order depths at relatively low computational cost, as in REFLEX and RESCUE (Arcorace et al., 2024; Pavesi et al., 2024); and (iii) the systematic use of satellite remote sensing, especially Sentinel-1 synthetic aperture radar (SAR), to derive event inventories for calibration, validation, and rapid post-event updating (e.g., Wagner et al., 2026), enabling more objective benchmarking and supporting operational services at continental and global scales.

At the same time, the limitations of purely topography-driven approaches are well-documented. The accuracy of DEM-based flood descriptors depends on the quality of the elevation data and its hydro-conditioning, such as sink filling/breaching, stream burning, and the representation of embankments and infrastructure, as well as the chosen algorithm. This is particularly true in very flat floodplains and urban environments. Furthermore, geomorphic outputs are generally most reliable when interpreted as flood susceptibility or flood-prone envelopes rather than event-specific hazard maps, as they do not explicitly address flow dynamics, hydraulic controls, or boundary conditions. River confluences remain challenging because flood-wave superposition and main-stem backwater can control tributary water levels and inundate secondary floodplains in ways that deviate from local drainage connectivity (Blöschl et al., 2013; Guse et al., 2020; Yan et al., 2024). Low-gradient outlets and coastal plains also present challenges. In morphodynamically active systems, planform changes (e.g., migration, widening, and avulsion) can relocate the active corridor and reactivate floodplain areas. Additionally, non-stationary hydroclimatic drivers challenge the “quasi-static” assumption implicitly embedded in morphology-only mapping.

This study presents an improved procedure, referred to as GFI 2.0, to address the limitations of the original GFI while preserving its operational simplicity and low data requirements that led to its widespread adoption. GFI 2.0 is specifically designed to enhance flood-prone delineation and depth estimation in intricate hydrogeomorphic settings. The core innovation is an iterative confluence module that refines the original GFI features to account for confluence-controlled backwater effects guided by stream hierarchy. We tested the methodology across 12 Italian basins using official ISPRA flood hazard maps and multiple DEM products. GFI 2.0 was also tested using a detailed hydraulic benchmark in the Bradano River basin based on two-dimensional simulations for 30-, 200-, and 500-year return periods. In this case, specific attention was paid to flood extent and water depth diagnostics.

1.1. A decade of geomorphic flood index development and applications

The GFI was developed based on a fundamental hydrological insight: flood dynamics leave distinct signatures in the terrain that can be extracted quantitatively from a DEM.

Since its early formulation, the index has been widely adopted for the rapid delineation of flood-prone areas, bridging the gap between complex hydraulic modelling and the pressing need for fast-processing and scalable flood hazard assessment tools (Manfreda et al., 2015; Samela et al., 2017a). Its most impactful use remains the delineation of flood-prone areas across large spatial scales, as demonstrated by the mapping of the entire continental United States (Samela et al., 2017b) and by a pan-European implementation via a web-based platform (Tavares da Costa et al., 2019). At the same time, the GFI has proven especially valuable in data-scarce contexts, where it provides an essential, terrain-based alternative to data-intensive hydrodynamic models.

Over the past decade, the GFI has been validated, refined and extended through a wide array of regional applications.

In Africa and Asia, especially in areas with limited data, the GFI has provided a first description of flood hazards (Samela et al., 2016; Faridani et al., 2020). Faridani et al. (2020) integrated GFI with IDF curves and hydrodynamic modelling (CADDIES-2D), enhancing the characterisation of flood dynamics in Iranian basins.

In eastern Asia, the GFI has been applied using both comparative and integrative approaches. For example, Talampas and Tarepe (2019) applied GFI with linear binary classifiers in the Philippines, achieving effective flood-prone area delineation despite minimal hydrological data. In Indonesia, it was combined with historical flood data to map hazard levels in the Kemuning watershed (Nugroho et al., 2019), and more recently benchmarked against HEC-RAS simulations in the Ciliwung River (Pratiwi et al., 2024). Further, Bintang (2024) introduced a modified GFI incorporating extreme rainfall indices, improving sensitivity to spatial rainfall variation. Hermon et al. (2024) employed the GFI in community-based flood resilience planning in Kampar Regency, further extending its scope beyond hazard mapping to support local adaptive strategies. A notable advancement was proposed by Abusarif et al. (2023), who modified GFI to account for tidal backwater effects in tropical rivers, improving flood prediction in coastal zones.

Applications in Mediterranean environments have also emerged. For instance, Deiana et al. (2023) leveraged high-resolution LiDAR data to apply GFI in small, morphologically complex catchments, refining floodplain characterisation. Galderisi et al. (2024) demonstrated GFI's practical utility in supporting local flood risk assessments and mitigation planning in inland, data-poor regions.

Across the globe, the GFI is now routinely validated as a reliable and cost-effective flood screening tool (Link et al., 2019; Magnini et al., 2022; Albertini et al., 2024; Virtriana et al., 2023; Salim et al., 2023).

It is also being used to perform targeted risk assessments for critical transportation infrastructure (Samela et al., 2023) and to map flood hazard in challenging environments like arid zones and even cliffed coastal regions (Albertini et al., 2022; Hamouda et al., 2024).

From this strong foundation, the GFI has grown into a remarkably adaptable tool, its narrative branching into numerous sector-specific applications. Researchers are continuously enhancing its capabilities by integrating the geomorphic logic with the predictive power of machine learning and deep neural networks (Tripathi and Mohanty, 2024; Mohanty and Tripathi, 2024; Balestra et al., 2022; Magnini et al., 2022; Gebrehiwot and Hashemi-Beni, 2022) and enriching it with other geographic inputs, such as land use, to refine its accuracy (Ferdiansyah et al., 2024; Yolina and Irwansyah, 2023). This evolution has unlocked a new tier of specialised applications, indicating that the GFI is increasingly recognised not only as a mapping tool but also as a useful framework for flood risk decision-making under different environmental and data conditions.

To further contextualise the global reach and disciplinary diversity of GFI studies, a spatial analysis was conducted using bibliometric data extracted from the Scopus database. To ensure relevance, the search query was carefully filtered using the keywords “GFI” and “flood”. This refined search yielded a total of 148 peer-reviewed documents that explicitly mention the GFI in flood-related research. The results were subsequently geocoded based on author affiliations and visualised in a global distribution map (Fig. 1), which illustrates the extent of GFI usage across regions. The United States, China, Italy, India, and Indonesia emerged as leading contributors, reflecting both academic interest and

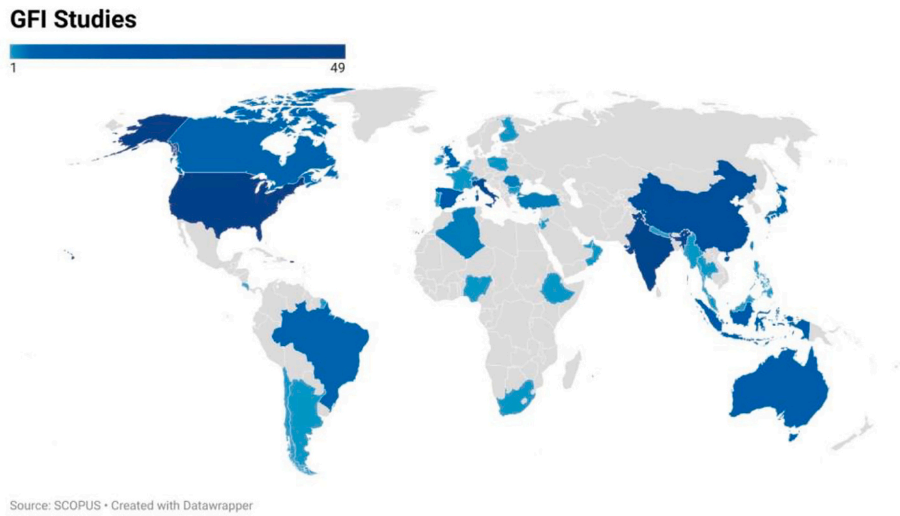

Fig. 1. Number of studies based on the use of GFI obtained from Scopus (last accessed on 05/03/2026).

the pressing nature of flood risk in these countries. This map not only highlights the widespread adoption of GFI in flood studies but also supports the subsequent thematic classification of the literature by revealing geographic clusters of methodological innovation and application.

1.2. Study objectives and contributions

This study builds on a decade of Geomorphic Flood Index (GFI) applications and recent progress in DEM-based hydro-geomorphic mapping. It consolidates and extends the GFI method into an enhanced operational framework, GFI 2.0, which is designed for the rapid, scalable delineation of flood-prone areas in regions with limited data. The proposed developments strengthen the physical consistency of morphology-driven flood susceptibility mapping while preserving the parsimony and computational efficiency that make the GFI attractive for large-area screening and supporting more data- and model-intensive analyses.

The objectives are twofold: (1) address the systematic limitations of GFI 1.0 in complex hydrogeomorphic settings, specifically the effects of confluence-controlled backwaters; (2) evaluate the implications of these refinements for mapping flood-prone areas and estimating first-order flood water depths when used in preliminary risk assessments and operational decision support.

Accordingly, the manuscript introduces a new GFI formulation that represents backwater influence based on stream hierarchy, followed by a systematic benchmarking against reference inundation maps. These maps are derived from two-dimensional hydrodynamic simulations in the Bradano River basin for multiple return periods. The manuscript also provides diagnostics on classification skill (flood extent) and depth-related performance and discusses computational efficiency, scale dependence, and practical use cases. These refinements position GFI 2.0 as a first-order screening tool that can be used as a standalone tool or as an interoperable layer in hybrid modelling strategies (e.g., focused hydraulic simulations) and machine learning/AI pipelines, where geomorphology can provide physically grounded predictors (e.g., Navarro et al., 2025).

2. Study basins, data and methods

2.1. Study basins and physiographic setting

To evaluate the performance and transferability of GFI 2.0 across contrasting hydrogeomorphic settings, 12 Italian river basins were selected. The basin sample spans a broad range of physiographic conditions, with drainage areas from 381 to 17,208 km^2, mean elevations from 316 to 1095 m a.s.l., and mean slopes from 7.5° to 18.8° (Table 1). Their geographic distribution across Italy is shown in Fig. 2. This sampling strategy was designed to capture variability in latitude, climate, topographic configuration, and basin morphology, thereby enabling a consistent large-scale assessment against nationally available reference flood maps.

In addition to the multi-basin comparison, a detailed case study was conducted for the Bradano River basin, for which a dedicated hydraulic simulation was developed. This basin was selected to further evaluate the ability of GFI 2.0 to reproduce flood spatial patterns at finer spatial detail.

The Bradano River basin (highlighted in red in Fig. 2) is one of the main river systems in Basilicata, southern Italy. The river is approximately 120 km long and drains 2997.52 km^2. The western and south-western sectors are predominantly mountainous, with elevations ranging from about 700 to 1250 m a.s.l. Downstream, the basin transitions into a hilly central sector, extending from the Forenza–Spinazzola area to the Matera–Montescaglioso area, where elevations generally range between 500 and 300 m a.s.l. The northeastern sector includes part of the Murge plateau, with elevations between about 600 and 400 m a.s.l. In its lower course, the Bradano crosses the Metaponto plain, traverses the Basilicata–Puglia border, and eventually discharges into the Ionian Sea near Metaponto.

2.2. Digital elevation data and reference flood maps

To evaluate the sensitivity of GFI 2.0 to topographic input data, the analysis was carried out using Digital Elevation Models (DEMs) from

Table 1
Main characteristics of the selected catchments.

Basin	Area (km^2)	Mean Elevation (m)	Mean Slope (°)
Bradano	2997.52	380.41	7.50
Flumendosa	1835.83	636.74	18.47
Garcia	950.10	421.89	9.64
North Po	17,207.54	1095.19	17.35
Ombrone	3564.18	315.67	10.77
Savuto	381.35	817.71	18.78
Simeto	4126.72	541.76	9.70
Tacina	420.63	622.36	14.47
Tanaro	9077.22	590.26	14.42
Tirso	3344.22	479.87	10.55
Trigno	1203.96	615.55	12.09
Volturno	6727.15	468.40	11.47

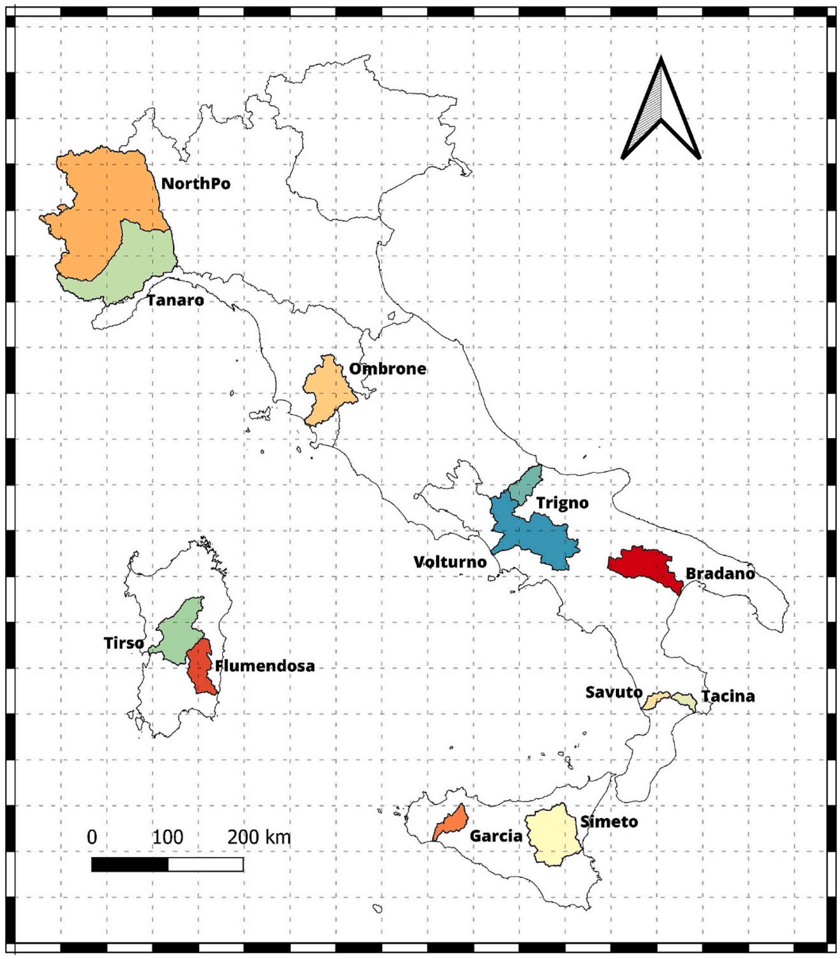

Fig. 2. Catchments selected for the assessment of the proposed modification to the GFI.

different sources and at different spatial resolutions. For the multi-basin assessment, three nominal resolutions were considered: 90, 30, and 10 m. In addition, because very high-resolution open-access DEMs are rarely available over large domains, a 5 m DEM was used only for the Bradano basin, where a more detailed local-scale analysis was performed.

The coarsest dataset adopted in this study is the Shuttle Radar Topography Mission (SRTM) DEM, used herein at approximately 90 m resolution. In its hydrologically conditioned HydroSHEDS version, SRTM provides near-global coverage and remains one of the most widely used freely available elevation datasets for large-scale hydrological and flood-related applications. Its extensive spatial coverage and standardised pre-processing make it a suitable benchmark for testing the robustness of DEM-based flood delineation methods under coarse-resolution conditions (Navarro et al., 2025; Albano et al., 2019; Manfreda et al., 2015; Annis et al., 2019). The second DEM used in this study is the Multi-Error-Remover Improved-Terrain (MERIT) at 3-arcsecond (~90 m) resolution (see Yamazaki et al., 2017). MERIT has proven to be highly reliable for hydrological applications and flood simulations (Hawker et al., 2018; Magnini et al., 2022). Being the product of multiple processing operations and corrections applied to previously available DEMs (i.e., NASA SRTM3 and JAXA AW3D), it eliminates critical errors—such as tree canopy height bias and sensor noise—that create "artificial dams" or flow blockages in other models.

At intermediate resolution, the analysis employed FABDEM, distributed at approximately 30 m resolution by the University of Bristol (Hawker et al., 2022). FABDEM is a global bare-earth DEM derived from Copernicus GLO-30 and corrected through a machine-learning procedure designed to reduce elevation biases associated with buildings and vegetation. Compared with conventional global DEM products, FABDEM generally provides a more realistic representation of terrain morphology in floodplain environments, and it has already been adopted in large-scale flood modelling applications (Wing et al., 2024; Hawker et al., 2024).

To ensure a consistent high-resolution analysis across all of Italy, TinItaly version 1.1 was used at 10 m resolution. Originally introduced by Tarquini et al. (2007), TinItaly was generated by mosaicking regional elevation datasets into a seamless national DEM. The most recent update corrected several artefacts and inconsistencies found in previous releases, improving its suitability for geomorphological and hydrological applications (Tarquini et al., 2023). Owing to its finer representation of local relief and drainage organisation, TinItaly provides an important reference for evaluating the effect of increasing DEM resolution on GFI performance (Annis et al., 2019; Magnini et al., 2022).

A high-resolution 5 m DEM was also available for the Bradano basin and was used exclusively for the detailed case study and the comparison with the two-dimensional hydraulic simulations. This additional dataset allowed us to investigate the behaviour of the method under very high-resolution topographic conditions, although its use could not be extended to the full national sample because comparable open-access data were not available for all basins.

For the large-scale assessment, the reference inundation data used for marginal area estimation, parameter calibration, and comparative evaluation were the official Flood Hazard Maps provided by ISPRA (2020 report; Lastoria et al., 2021). These maps classify inundated areas into three hazard categories: High Probability Hazard (HPH), associated with relatively frequent floods with return periods of approximately 30-50 years; Medium Probability Hazard (MPH), associated with return periods of 100 to 200 years; and Low Probability Hazard (LPH), associated with rare events with return periods exceeding 200 years. The adoption of ISPRA maps ensured a consistent and standardised national benchmark across all investigated basins while maintaining a balance between spatial coverage, data availability, and computational feasibility.

2.3. Two-dimensional hydraulic modelling in the Bradano basin

The performance of GFI 2.0 was evaluated against flood maps generated through two-dimensional (2D) hydrodynamic simulations performed with HEC-RAS 5.0.7. The hydraulic model was implemented for the areas downstream of the San Giuliano dam under unsteady flow conditions. Three flood scenarios with return periods of 30, 200, and 500 years were considered. Peak discharges were estimated using the regional VAPI ("Valutazione delle Piene in Italia") method (Rossi and Villani, 1998), and the corresponding values are reported in Table 2.

Synthetic hydrographs were constructed from peak discharges following the formulation proposed by Fiorentino (1985), which assumes a symmetric hydrograph with exponential limbs. These hydrographs are depicted in Fig. 3.

To implement the 2D flow area, a DEM with a resolution of 5 m was used. This was projected in the Universal Transverse Mercator (UTM) projection method to the EPSG:32633 – WGS 84 / UTM zone 33 N coordinate reference system. The computational mesh was defined as variable-sized square cells to ensure greater computational efficiency, with a base size of 50 m × 50 m (see Fig. 4). This mesh was then densified using 'breaklines', which correspond to the fundamental elements required for modelling existing levees, crossed infrastructures and the riverbed. The mesh size of these elements is 20 m × 20 m (see Fig. 4). Two roughness regions were defined within the model domain. A Manning's coefficient of 0.033 s $m^{-1}/^{3}$ was assigned to the main channel, while a value of 0.045 s $m^{-1}/^{3}$ was adopted for overbank floodplain areas. Two boundary conditions were assigned to the computational area: an upstream 'Flow Hydrograph' condition, imposed at the inlet of the 2D flow area; and a downstream 'Normal Depth' condition applied near the river mouth, assuming an energy slope of 0.02 consistent with the local riverbed gradient. The model configuration follows previous engineering studies conducted for the same river reach (Pacia et al., 2023), where further details regarding this hydraulic modelling exercise can be found. Due to the lack of continuous observed water level data in the downstream section, the model was not calibrated against measured flood events and is therefore used as a physically-based benchmark for comparative purposes.

The simulations were carried out with a computational time step of 5 s. Output results were stored at 1-h intervals over a total simulation duration of 177 h for each scenario. The reference maps used for the final validation of the GFI 2.0 approach correspond to the maximum water depth envelope obtained during non-stationary events.

The hydraulic simulations highlight a clear spatial variability of flood behaviour along the analysed reach. The section immediately downstream of the San Giuliano Dam, extending for about 4 km upstream of the SP2 crossing, is well confined within the channel and shows no signs of flooding.

Between the SP2 and SS106 crossings, flooded areas are limited to zones immediately adjacent to the river corridor in all three flow conditions, presumably due to the terrain's morphological configuration in that area. In contrast, a broader expansion of flooded areas is observed in the section downstream of the SS106 highway crossing, likely due to the flatter topography allowing for greater spreading of the water flow.

The maximum water depth maps derived from these simulations constitute the benchmark dataset used to assess the performance of GFI 1.0 and GFI 2.0.

Table 2
Flood peaks estimated with the regional method at return periods of 30, 200, and 500 years.

$Q_{30\ Years}$ [m^3/s]	$Q_{200\ Years}$ [m^3/s]	$Q_{500\ Years}$ [m^3/s]
1770	3375	4070

2.4. GFI 2.0 methodological framework

The GFI, first introduced by Manfreda et al. (2015) and Samela et al. (2017a); Samela et al. (2017b), is a basin-scale composite index representing the ratio between two geomorphic features (eq. 1): (i) the water depth of the river nearest to the point of interest (h_r, eq. 2) and (ii) the elevation difference between the point of interest and the closest river channel (H).

$$\mathrm{GFI} = \ln(\mathrm{h_r}/\mathrm{H}) \tag{1}$$

The h_r variable in Eq. 1 is derived from a hydraulic scaling relationship proposed by Leopold and Maddock (1953):

$$\mathrm{h_r} \approx \mathrm{a}^{*}\mathrm{A_{river}}^{\mathrm{n}} \tag{2}$$

where A_{river} (km^2) is the upslope contributing area, a is a scaling factor, and n is a dimensionless exponent. The two parameters can be calibrated using data from monitoring stations. In areas where little or no information is available, it is possible to define a as 1 and n as 0.354, the latter of which corresponds to the average of different values extracted from the literature (see Samela et al., 2018). By performing a thresholding of the index through a linear binary classification using flood hazard reference maps (e.g., flood maps for specified return period), flood-prone areas can be identified.

The improved version, referred to as GFI 2.0, introduces an iterative procedure designed to account for the influence of large floods occurring in the main river, which may also affect areas directly drained by secondary tributaries near confluences.

The overall workflow of the GFI 2.0 is summarised in Fig. 5. The first step involved computing the original GFI (hereafter GFI 1.0) in the basin, and an initial estimation of flood-prone areas, the classification threshold (τ) and flood water depth (WD 1.0) based on the comparison with the flood hazard map (see Samela et al., 2017a; Samela et al., 2017b for more details on the original procedure).

In the second step, the GFI 1.0 was iteratively refined to account for the influence of river confluences,yielding a new flood water depth estimate (WD 2.0).

2.4.1. Flood extent classification and performance metrics

In the present study, a linear binary classification was employed to distinguish flooded from non-flooded areas via a linear boundary represented by a threshold value (τ), which was applied to the GFI index.

The min-max normalisation was applied to rescale the GFI matrix in the range − 1 to 1. Consequently, a normalised threshold that transforms the normalised GFI matrix into a binary map of potential flood-prone areas is determined by minimising the sum of two performance metrics, i.e., the False Positive Rate (R_{FP}, overestimation) and the False Negative Rate (R_{FN}, underestimation), thereby assigning equal weights to both rates.

To ensure a robust global validation of the model, the analysis was further strengthened by incorporating the Cohen's Kappa index and the Critical Success Index (CSI). The Kappa index was utilised to assess the overall reliability of the classification by measuring the agreement between the predicted and observed flooded areas while strictly accounting for chance agreement. Concurrently, the CSI (also known as the Threat Score) was employed to provide a comprehensive evaluation of the model's accuracy, effectively penalising both false alarms and missed flood events. Additionally, the performance of the classifiers was compared using the Receiver Operating Characteristics (ROC) curve and

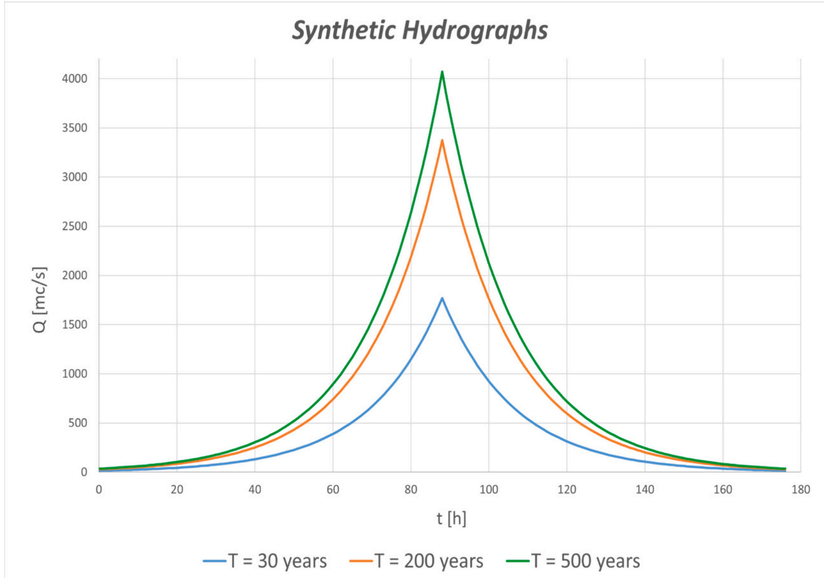

Fig. 3. Synthetic hydrographs constructed for the peak flow values for the three different return periods, T, of 30, 200, and 500 years.

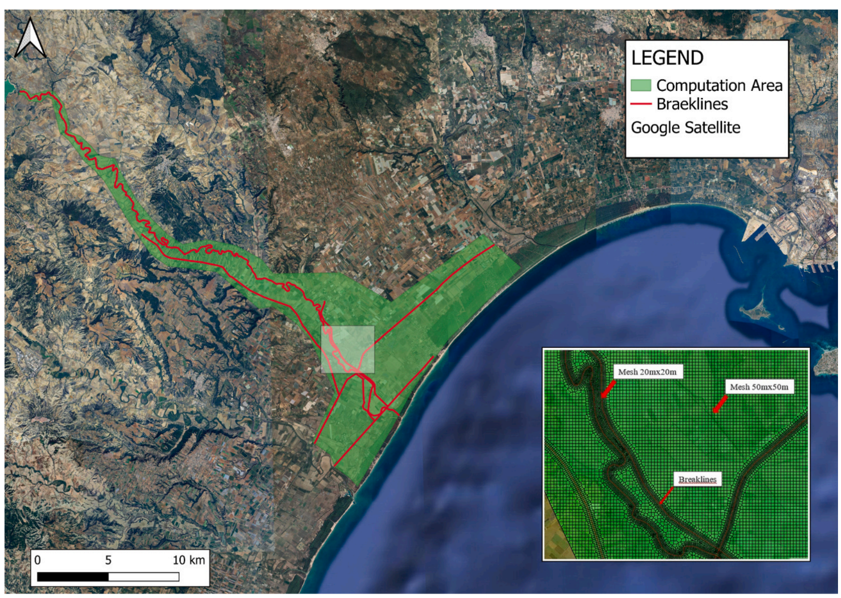

Fig. 4. Extent of the defined two-dimensional flow area, and detail of the computational mesh used, showing the breaklines introduced to account for the presence of riverbanks.

the Area under the ROC Curve (AUC) (Fawcett, 2006). The AUC ranges from 0.5 (completely random classifier) to 1 (perfectly discriminating classifier).

To evaluate the influence of macro-topography on the effectiveness of GFI 2.0, a stratified analysis was performed at the basin-scale. Each of the twelve catchments was categorised into one of three physiographic classes based on its mean elevation (Z):

- Valley (Z $<$ 300 m a.s.l.),
- Hillslope (300 $<$ Z $<$ 600 m a.s.l.),
- Mountain (Z $>$ 600 m a.s.l.).

Performance metrics were then aggregated within these classes to identify systematic behaviours linked to regional topographic gradients.

2.4.2. Flood-depth estimation from GFI

The GFI definition was also used for flood water depth analysis (hereinafter referred to as *WD*). Manfreda and Samela (2019) introduced an estimation method of the parameter *a* based on the following equation:

$$a = 1/\exp(\tau) \tag{3}$$

where τ corresponds to a threshold value derived from a linear binary classification, allowing *WD* to be as follows:

$$WD = h_r - H \tag{4}$$

2.4.3. Iterative confluence module

Flooding at a river confluence is more likely to be controlled by the main river than the tributaries. Therefore, the Confluence module was developed to iteratively refine GFI 1.0 to account for this backwater

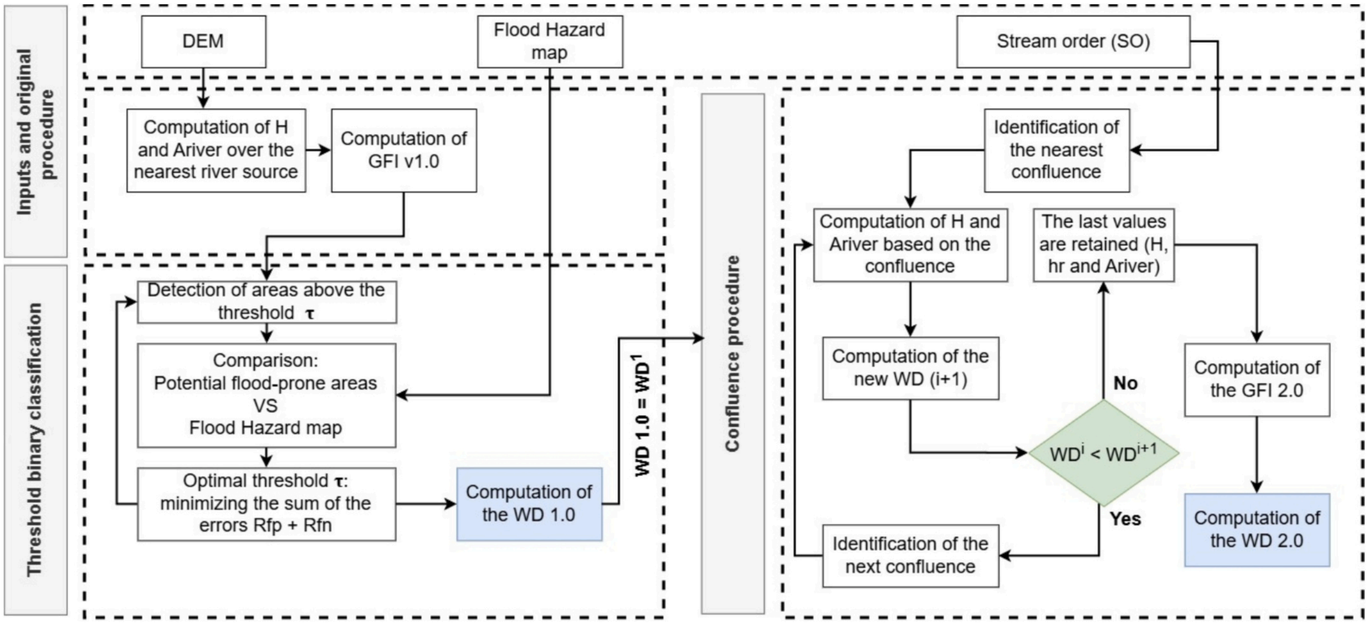

Fig. 5. Methodological workflow for delineating flood-prone areas using the new Geomorphic Flood Index (GFI 2.0).

effect within the tributary sub-basin.

Within the code, confluences are identified using the Horton-Strahler classification of individual reaches. This method is widely used to classify the hierarchy of streams within a river network. It helps to assign an order to streams, with the smallest, unbranched tributaries being designated as first-order streams. When two first-order streams converge, they form a second-order stream. Similarly, when two second-order streams converge, they create a third-order stream, and so on. If a stream of one order joins a stream of a higher order, the higher order is retained (Horton, 1945; Strahler, 1952, 1957).

The module compares the geomorphic feature values computed for each pixel (related to the nearest river) with those of the nearest identified confluence downstream of the given point. Specifically, for any given pixel, the procedure first identifies the nearest confluence and then computes the h_r, H and water depth (WD 2.0). This new depth estimate is then compared with the estimate derived from the GFI 1.0. If the WD 2.0 is greater than WD 1.0, the original h_r and H values (e.g. $i = 1$, nearest river) are replaced with the confluence values (see Fig. 6). If a second confluence is nearby, the process is repeated iteratively, stopping when the confluence between a tributary and the main river is reached, or when the WD condition is not satisfied. Once the iteration process is completed, GFI 2.0 is executed and calibrated to estimate the new parameter *a* for retrieving the final WD map.

2.4.4. Evaluation metrics for flood-depth estimates

GFI 2.0 performances were assessed for both flood extent (Section 2.3.2) and flood water depth for each return period (30, 200 and 500 years). The performance of flood water depth was evaluated based on mean square error (MSE), root mean square error (RMSE), Kling–Gupta efficiency (KGE), and the linear correlation coefficient (r). Additional statistical measures were computed to enhance the understanding of the changes in GFI, including mean, median, maximum, minimum, Interquartile range (IQR), and variance.

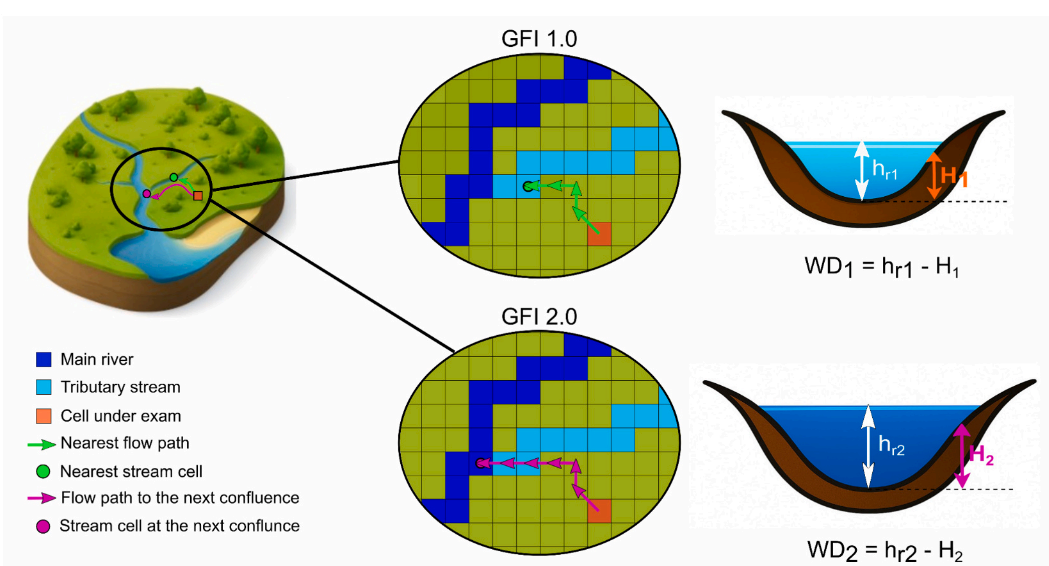

Fig. 6. Graphical representation of the feature selection operated by the confluence module (GFI 2.0).

3. Results

The analysis is organised into two main components: (i) a broad assessment of the model's transferability across twelve different geographical environments and Digital Elevation Model (DEM) resolutions, and (ii) an in-depth evaluation of the confluence iteration procedure conducted on the Bradano River basin to analyse the specific improvements in flood extent and water depth estimation.

3.1. Multi-basin assessment across geomorphological settings

To evaluate the robustness and transferability of the proposed methodology, GFI 2.0 was tested across a national sample of twelve Italian basins. This selection covers a diverse range of hydro-geomorphic contexts, from wide alluvial plains to confined mountainous catchments. For each basin, the comparison with ISPRA flood hazard maps provided a consistent benchmark for evaluating the relative performance of the baseline formulation (GFI 1.0) against the revised backwater-aware configuration (GFI 2.0) under different geomorphological and topographic conditions. As shown in Fig. 7, model performance is strongly influenced by DEM resolution. Across the four DEM products, CSI and Kappa generally increase as the DEM resolution becomes finer, whereas AUC remains high and comparatively stable across scenarios and model configurations. The advantage of GFI 2.0 is most pronounced when coarser DEMs are used, as the confluence correction partially compensates for the loss of local topographic detail and improves the spatial coherence of the mapped inundation. When 30–10 m DEMs are used, the performance gap between GFI 1.0 and GFI 2.0 becomes smaller, suggesting that high-resolution terrain data already captures part of the floodplain connectivity that the confluence module explicitly introduces.

The stratified analysis by geomorphological class (Fig. 8) further clarifies the contexts in which the revised formulation is most effective.

- Valley environments show the highest overall skill, with consistently higher CSI and Kappa values and relatively limited dispersion among basins.
- Hillslope catchments also benefit from the GFI 2.0 formulation, although with greater inter-basin variability.
- In contrast, mountainous basins display a marked reduction in predictive skill for both model versions, together with broader metric distributions and only marginal differences between GFI 1.0 and GFI 2.0. This pattern indicates that the confluence module is most beneficial where floodplain expansion and tributary–main stem interactions exert a stronger control on inundation patterns, whereas its contribution is more limited in steep and strongly confined settings.

Overall, the multi-basin analysis confirms that GFI 2.0 preserves the general behaviour and operational simplicity of the original formulation while extending its applicability to hydrodynamically more complex environments. The revised method is therefore particularly advantageous for regional-scale screening in large low-gradient river systems and for applications based on medium- to coarse-resolution DEMs, whereas in steep and strongly confined basins the simpler GFI 1.0 remains a competitive approximation.

3.1.1. Executions time

GFI 2.0 was designed to remain computationally efficient and scalable across DEM resolutions, enabling basin-to-regional screening at a fraction of the cost typically associated with 2D hydrodynamic modelling. To quantify runtime and identify computational bottlenecks, we profiled the full GFI workflow over the North Po basin (≈17,400 km^2) using four DEM products spanning 90 m to 10 m resolution. For each configuration, we report the wall-clock time of the main processing blocks: (i) hydro-conditioning, (ii) computation of topological distances,

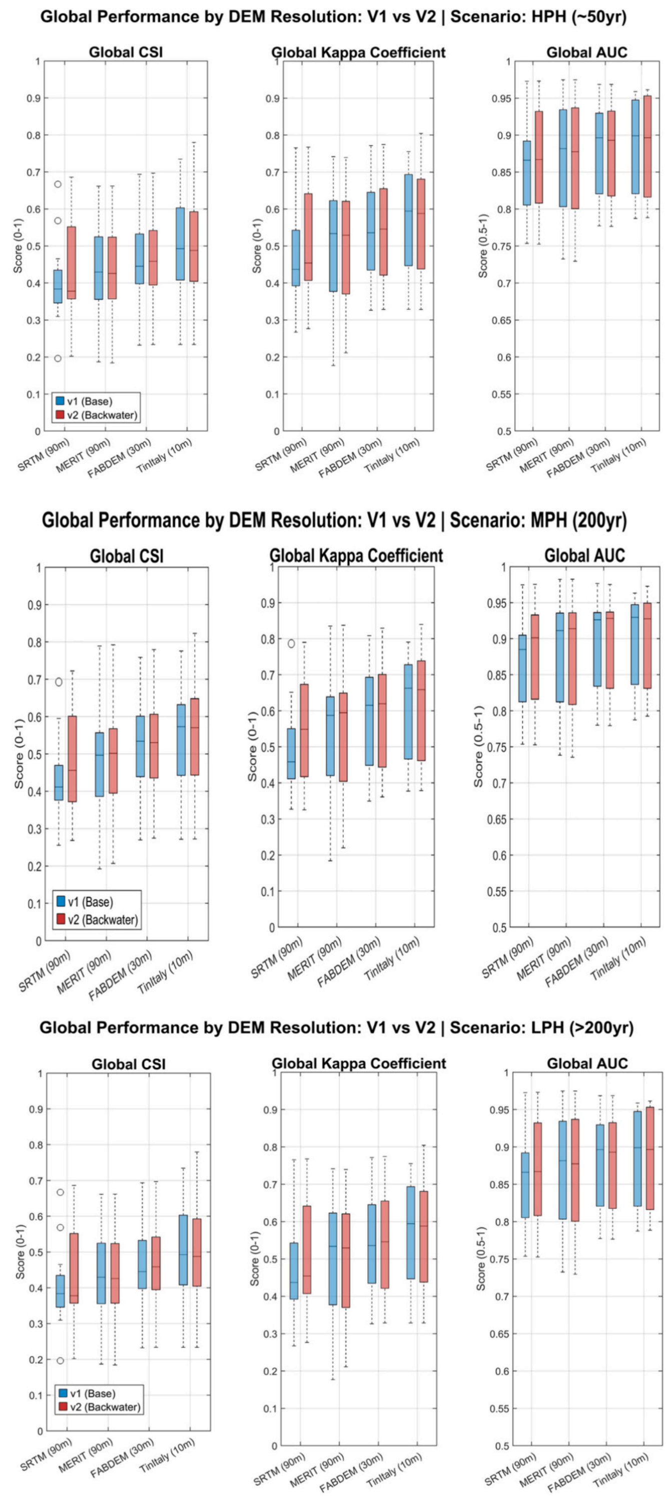

Fig. 7. Comparison of the overall performance of the two model configurations, V1 (Base) and V2 (Backwater), as a function of DEM resolution for the three scenarios HPH (~50 years), MPH (200 years), and LPH (>200 years). The boxplots show the distribution of CSI, Kappa coefficient, and AUC scores for four DEMs: SRTM (90 m), MERIT (90 m), FABDEM (30 m), and TinItaly (10 m). Overall, CSI and Kappa tend to increase with finer resolution DEMs, while AUC remains high and relatively stable across scenarios and model versions.

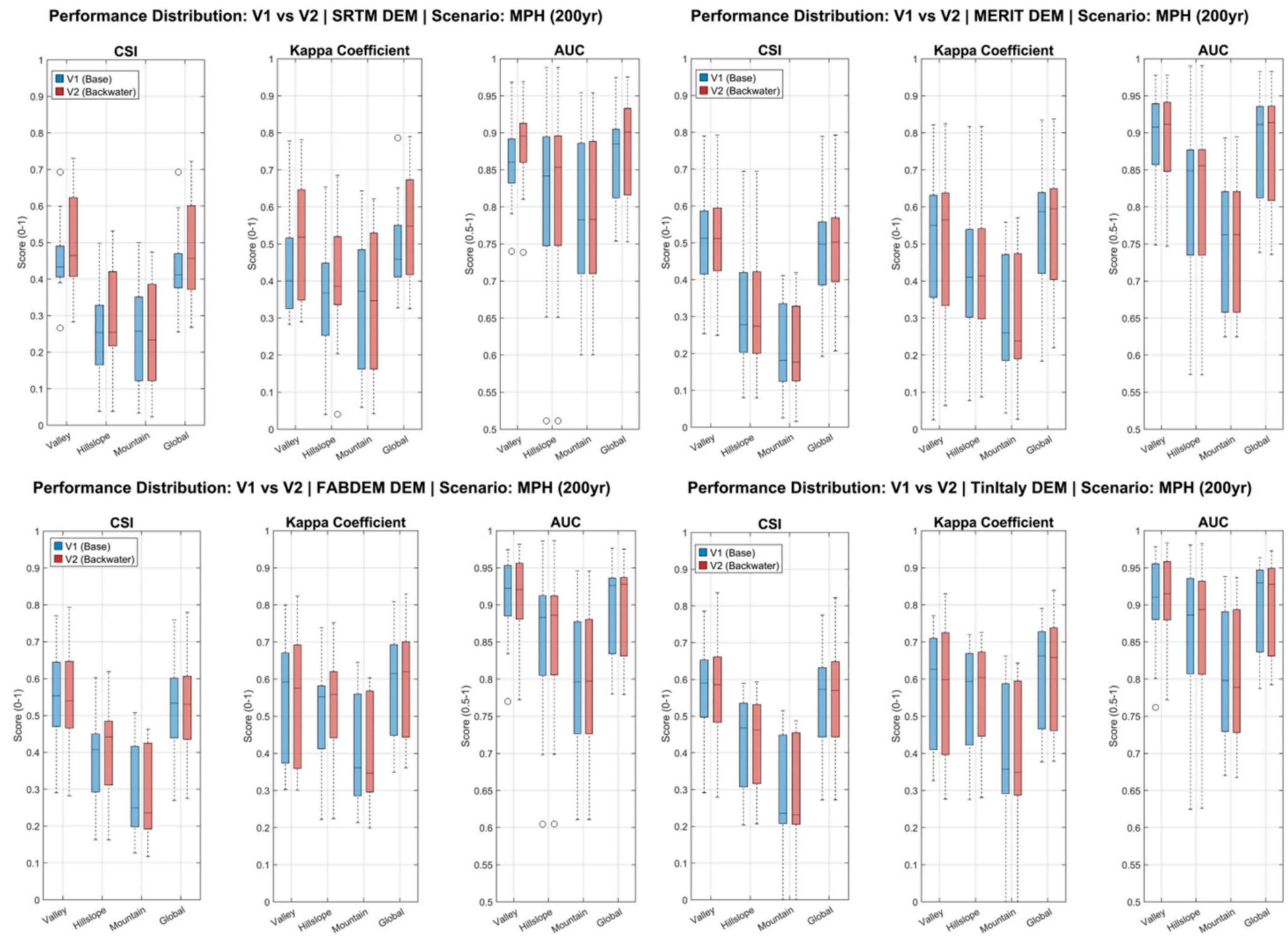

Fig. 8. Comparison of the overall performance of the two model configurations, V1 (Base) and V2 (Backwater), as a function of mean elevation of the reference areas which are distinguished in valley (elevation <300 m asl), hillslope (300 < Z < 600 m asl), mountain (Z > 600 m asl) specifically for the intermediate scenario MPH (200 years). The boxplots show the distribution of CSI, Kappa coefficient, and AUC scores for four DEMs: SRTM (90 m), MERIT (90 m), FABDEM (30 m), and TinItaly (10 m).

(iii) calibration of the original GFI (v1.0) parametrisation, (iv) the GFI 2.0 topological backwater propagation, and (v) the final recalibration step required by the updated framework (Table 3).

Overall runtimes increase with the number of basin pixels, yet remain within operational limits even at high resolution. At 10 m (TinItaly), the basin comprises ~173.9 million pixels and the complete execution required 3771 s (≈62.9 min). At 30 m (FABDEM), the full run completes in 459 s (≈7.6 min), while at 90 m runtimes are approximately 1.0 min for both DEM products adopted (MERIT vs SRTM).

Importantly, the newly introduced topological backwater propagation is highly optimised and contributes only a negligible fraction of the total runtime across all resolutions. Even at 10 m, the backwater module required **9.26 s**, corresponding to **<0.3%** of the total runtime; at coarser resolutions it remained well below 2 s. Consequently, the overall computational cost is dominated by (a) the computation of topological distances and (b) calibration/recalibration steps, while the added physical realism introduced by the confluence-aware propagation is achieved with minimal computational overhead.

3.2. *Detailed assessment in the Bradano basin*

A detailed evaluation was conducted on the Bradano River basin to examine how the confluence module modifies the original GFI formulation and affects the delineation of flood-prone areas. For each return period (30, 200, and 500 years), GFI 1.0 was first computed and then updated through the iterative confluence procedure. ROC analysis shows a systematic improvement in classification skill for the revised formulation. Specifically, AUC increased from 0.917 to 0.952 for the 30-year scenario, from 0.918 to 0.960 for the 200-year scenario, and from 0.914 to 0.959 for the 500-year scenario. The same trend is reflected in

Table 3
Runtime breakdown of the GFI 2.0 workflow for the North Po basin across DEM products and resolutions.

DEM source	Res. (m)	Total pixels	Basin pixels	Hydro-conditioning (s)	Topological distances (s)	v1.0 calibration (s)	v2.0 backwater (s)	v2.0 recalibration (s)	Total execution (s)
SRTM_90m	90	4,836,240	2,661,131	3.78	7.50	22.86	0.21	23.56	57.91
MERIT_90m	90	4,836,240	2,671,354	3.28	7.77	23.88	0.18	24.27	59.38
FABDEM_30m	30	44,608,000	24,546,302	31.41	99.02	160.26	1.58	166.39	458.67
TinItaly_10m	10	319,144,836	173,869,094	278.05	1408.12	1001.40	9.26	1074.26	3771.09

the true positive rate, which increased from 0.839 to 0.948, from 0.826 to 0.929, and from 0.825 to 0.928, respectively. False positive rates remained broadly comparable overall, with only a slight increase for the 30-year scenario and small reductions for the two larger return periods.

The improvement is also evident in the combined classification error, $R_{FP} + (1 - R_{TP})$, which decreased from 0.239 to 0.141 for $T = 30$ years, from 0.283 to 0.174 for $T = 200$ years, and from 0.288 to 0.183 for $T = 500$ years. The optimal normalised threshold (see Table 3) remained unchanged for the 30-year scenario (−0.300), whereas it shifted slightly for the 200- and 500-year events, from −0.350 to −0.325 and from −0.355 to −0.330, respectively. These threshold variations also translate into different calibrated values of parameter *a*, which is subsequently used for flood water-depth estimation.

Although the iterative correction affected only a limited fraction of the basin, its effect on the final flood maps is substantial. The proportion of cells modified by the confluence module was 0.97% for $T = 30$ years, 2.28% for $T = 200$ years, and 2.45% for $T = 500$ years. These cells are concentrated near confluences, where local drainage connectivity alone is insufficient to represent the hydraulic influence of the main stem. In these sectors, replacing the original descriptors with confluence-based values produces a flood pattern that more closely matches the hydraulic benchmark, while leaving the rest of the basin largely unchanged.

The spatial patterns shown in Figs. 9–11 are consistent with the quantitative metrics. The confluence module identifies a limited number of strategically located sectors for iteration, and the resulting GFI 2.0 flood maps show a closer correspondence with the hydraulic reference than the original formulation, particularly in the zoomed confluence areas and in the downstream low-gradient reaches. This confirms that the gain in overall performance is not due to a diffuse modification of the basin, but to a targeted correction of hydrodynamically sensitive areas.

3.2.1. *Flood-depth estimation in the Bradano basin*

The Bradano application also allows a direct assessment of the flood water-depth estimates derived from the two GFI formulations against the two-dimensional hydraulic simulations. As expected from a geomorphic approach, GFI-based depth maps do not reproduce the full dynamics of unsteady flow, but they do provide a first-order estimate of the spatial distribution of inundation depth. In line with the original analysis, GFI-derived depths generally tend to exceed the simulated values; however, GFI 2.0 reduces this discrepancy, especially for the larger return periods. Table 4 and Table 5 report the metrics for the different return period scenarios under the original and revised GFI formulation.

For the 30-year scenario, the improvement is modest but still visible, with MSE decreasing from 4.08 to 3.83 and RMSE from 2.02 to 1.96 m, while the linear correlation increases from 0.64 to 0.67. In contrast, the Kling–Gupta efficiency decreases slightly from 0.57 to 0.53, indicating that the two formulations perform similarly for the more frequent flood. The benefits of GFI 2.0 become much more evident at $T = 200$ and $T = 500$ years. At $T = 200$ years, RMSE decreases from 5.25 to 3.24 m, KGE increases from −0.27 to 0.26, and correlation rises from 0.42 to 0.51. At $T = 500$ years, RMSE decreases from 5.66 to 3.58 m, KGE increases from −0.24 to 0.22, and correlation improves from 0.39 to 0.46.

The revised formulation also reduces the positive bias that characterises the GFI 1.0 depth estimates. For the 200-year event, mean depth decreases from 6.88 to 5.21 m, moving closer to the simulated average of 3.37 m; for the 500-year event, it decreases from 7.42 to 5.73 m, compared with a simulated mean of 3.72 m. A similar contraction is observed in the distribution of depths, with lower medians, interquartile ranges, and variances. For example, at $T = 200$ years the IQR decreases from 6.05 to 3.66 m and the variance from 17.09 to 6.26, while at $T = 500$ years the IQR decreases from 6.17 to 3.64 and the variance from 19.27 to 6.47. These results indicate that GFI 2.0 not only reduces average error, but also yields a more stable and spatially coherent depth distribution.

The map comparison for the 200-year scenario (Fig. 12) is consistent with the statistical analysis, showing that GFI 2.0 produces flood water-depth patterns that are less fragmented and closer to the hydraulic reference than those obtained with GFI 1.0. Overall, the Bradano case study confirms that the confluence module improves both flood-extent classification and first-order depth estimation, with the strongest benefits emerging under the more extensive flood scenarios.

4. Discussion and implications

The results indicate that the main value of GFI 2.0 is not a uniform increase in skill under all conditions, but a process-based correction of the situations in which GFI 1.0 is structurally weakest, namely river

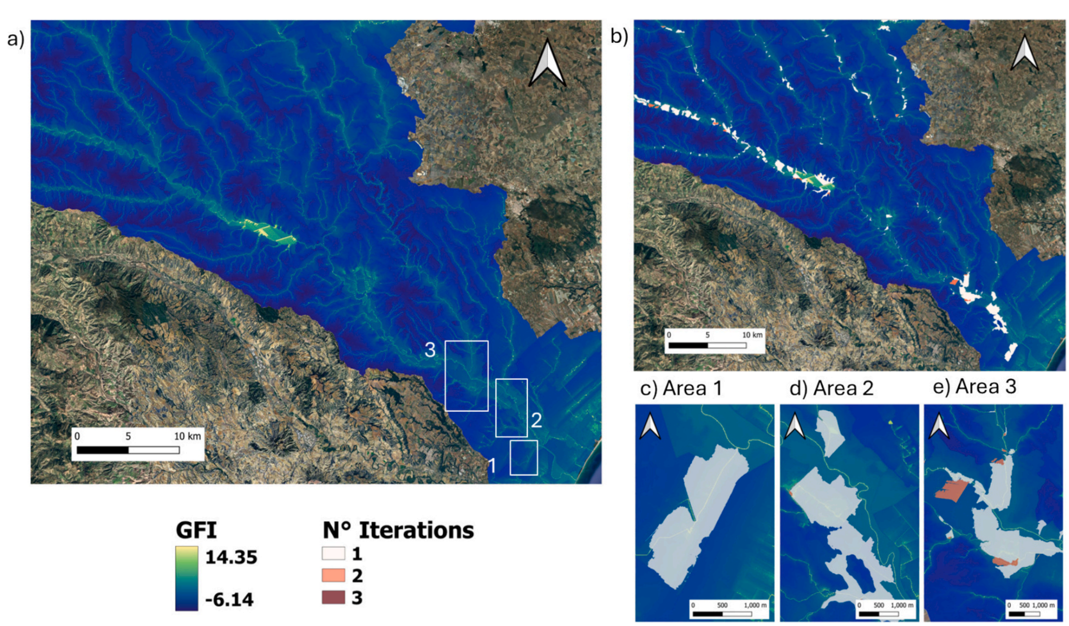

Fig. 9. Geomorphic Flood Index (GFI) version 1.0, calculated in the basin and adjacent areas at coastal outlets. Also, areas identified in the confluence module as requiring iteration. a) GFI 1.0; b) Number of iterations over the identified areas; c), d) and e) Three zoomed-in areas within the relevant confluence zone are included to enhance understanding of the iterated areas.

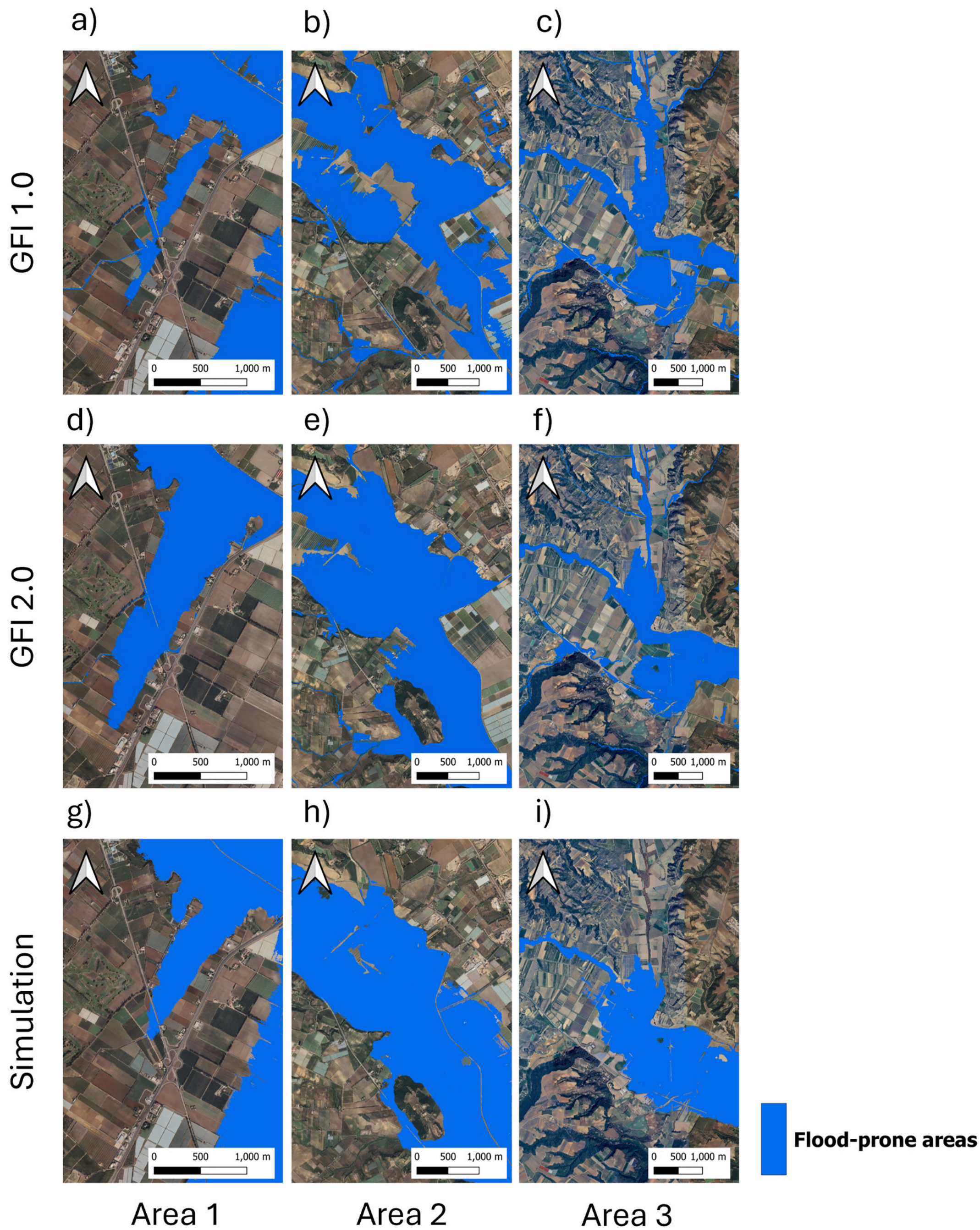

Fig. 10. Extent of the flood-prone areas based on $T = 200$ years. a-c) GFI 1.0. d-f) GFI 2.0. g-i) Hydraulic simulation.

confluences, low-gradient floodplains, and wide valley bottoms. In these settings, inundation is controlled not only by the nearest drainage line and local relief, but also by downstream water-level controls, backwater propagation, and tributary-main stem interactions. By explicitly representing these effects through an iterative confluence procedure, GFI 2.0 improves the hydraulic plausibility of DEM-based flood mapping while preserving the simplicity of the original framework.

The Bradano application clearly illustrates this mechanism. Although the confluence module modified only a small fraction of basin cells (0.97–2.45% depending on return period), the resulting improvement in flood extent delineation was systematic: AUC increased to 0.952, 0.960, and 0.959 for the 30-, 200-, and 500-year scenarios, respectively, while the combined classification error declined markedly. This confirms that confluence-sensitive sectors, even when spatially limited, can exert a disproportionate control on the realism of the mapped inundation pattern.

The multi-basin assessment clarifies the domain of validity of the revised formulation. The largest gains occur in valley and hillslope environments and, more generally, in large low-gradient systems where tributary-main stem interactions influence local inundation. By contrast, improvements are smaller in steep and strongly confined mountainous basins, where valley geometry already constrains flood spreading and GFI 1.0 captures most of the relevant topographic signal. GFI 2.0 should therefore be interpreted as a targeted refinement of the original index rather than as a universal replacement.

An equally important outcome concerns computational performance. The runtime analysis for the North Po basin (~17,400 km^2) shows that the complete GFI 2.0 workflow remained operationally lightweight across all DEM resolutions: 59–117 s for the 90 m products, 459 s (7.6 min) for FABDEM at 30 m, and 3771 s (62.9 min) for TinItaly

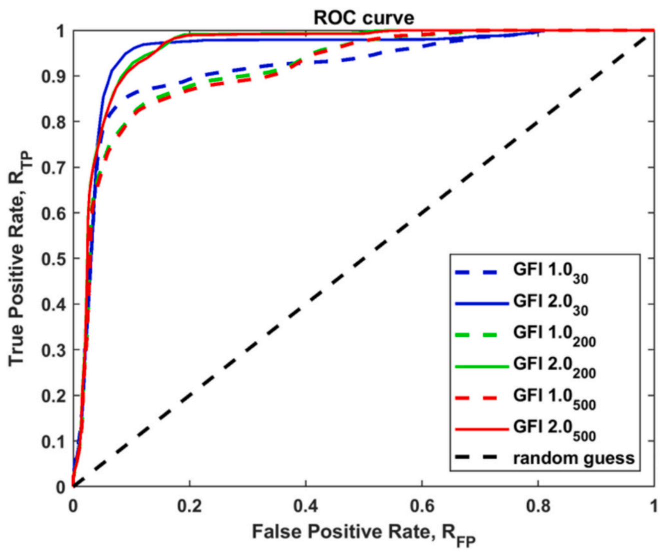

Fig. 11. ROC curves of GFI 1.0 and GFI 2.0 with respect to hydraulic simulations for return periods of 30, 200, and 500 years.

at 10 m, despite the 10 m configuration involving ~174 million basin pixels. Crucially, the new backwater-propagation step required only 0.18–0.21 s at 90 m, 1.58 s at 30 m, and 9.26 s at 10 m, i.e., less than 0.3% of the total runtime even in the most demanding case. The dominant computational costs remain the topological-distance calculation and the calibration/recalibration steps, meaning that the added physical realism of GFI 2.0 is obtained with negligible extra overhead.

These runtime results help interpret the role of DEM resolution. The national-scale comparison indicates that the relative advantage of GFI 2.0 is greater when coarse DEMs are used, because the confluence module partly compensates for the missing local topographic detail by introducing additional process representation. At the same time, the computational burden grows predictably with resolution, so the method offers a practical trade-off: coarse and medium-resolution DEMs enable very rapid screening over large regions, whereas 10 m products remain feasible for more detailed basin-scale applications while still preserving an operational workflow for screening studies.

The comparison of flood water depths leads to a similar but more nuanced interpretation. GFI 2.0 improves first-order depth estimates, especially for the 200- and 500-year scenarios, where backwater effects and floodplain storage become more influential. Nevertheless, these depth maps should not be interpreted as dynamic hydraulic outputs. The method does not solve flow momentum, reproduce hydrograph timing or velocities, or explicitly represent levees, culverts, bridges, or other engineered controls. These limitations remain particularly relevant in very flat floodplains, densely engineered corridors, and urban areas.

A further consideration concerns the benchmark datasets used for validation. ISPRA hazard maps provide a robust national-scale reference, but they are regulatory hazard layers rather than observations of individual events. Likewise, the Bradano benchmark is based on physically meaningful two-dimensional simulations but not on observed flood extents or water levels. The improvements reported here should therefore be interpreted primarily as evidence of consistent relative gains over GFI 1.0. Future work should extend validation against satellite-derived flood footprints, post-event surveys, and observed stage data. Overall, the proposed methodology represents a substantial step forward in hydro-geomorphic flood mapping. GFI 2.0 retains the parsimony, scalability, and limited data requirements that made the original GFI attractive, while extending its applicability to hydrodynamically complex settings that are difficult to capture with morphology-only approaches. The combination of better performance in confluence-dominated areas and negligible additional runtime makes the method particularly suited to regional screening, preliminary hazard assessment, and hybrid workflows in which geomorphic predictors support hydraulic simulations, remote sensing analyses, or machine-learning models in data-scarce regions.

5. Conclusions

This study presented GFI 2.0, an enhanced version of the Geomorphic Flood Index specifically developed to address one of the main limitations of DEM-based flood mapping: the inability of purely geomorphic methods to represent confluence-controlled backwater effects. By introducing an iterative correction guided by stream hierarchy, the proposed formulation improves the physical consistency of inundation mapping while preserving the low data requirements and practical simplicity of the original framework.

Table 4
Values of the optimal normalised thresholds and relative performance measures obtained in calibrating the linear binary classifiers on the Bradano River.

		τ	rfp	rtp	rfp + (1-rtp)	AUC	real τ	a
T = 30 years	GFI 1.0	−0.300	0.078	0.839	0.239	0.917	0.744	0.475
	GFI 2.0	−0.300	0.089	0.948	0.141	0.952	0.744	0.475
T = 200 years	GFI 1.0	−0.350	0.109	0.826	0.283	0.918	0.221	0.802
	GFI 2.0	−0.325	0.102	0.929	0.174	0.960	0.482	0.617
T = 500 years	GFI 1.0	−0.355	0.113	0.825	0.288	0.914	0.168	0.845
	GFI 2.0	−0.330	0.111	0.928	0.183	0.959	0.430	0.650

Table 5
Performance metrics of water depth (WD) estimates derived from GFI 1.0 and 2.0 against hydrodynamic simulations across return periods of 30, 200, and 500 years.

	T = 30 years			T = 200 years			T = 500 years		
WD	Simulation	GFI 1.0	GFI 2.0	Simulation	GFI 1.0	GFI 2.0	Simulation	GFI 1.0	GFI 2.0
MSE	–	4.08	3.83	–	27.56	10.48	–	32.06	12.80
RMSE	–	2.02	1.96	–	5.25	3.24	–	5.66	3.58
KGE	–	0.57	0.53	–	−0.27	0.26	–	−0.24	0.22
Correlation	–	0.64	0.67	–	0.42	0.51	–	0.39	0.46
Mean	2.29	2.82	3.06	3.37	6.88	5.21	3.72	7.42	5.73
Median	1.50	2.64	2.84	2.18	7.97	5.15	2.33	8.67	5.69
Maximum	11.14	8.08	8.08	14.55	13.64	10.50	16.15	14.37	11.06
Minimum	0.00	0.00	0.00	0.00	0.00	0.00	0.00	0.00	0.00
IQR	3.12	4.25	3.75	4.20	6.05	3.66	4.60	6.17	3.64
Variance	4.96	5.58	4.98	8.04	17.09	6.26	9.57	19.27	6.47

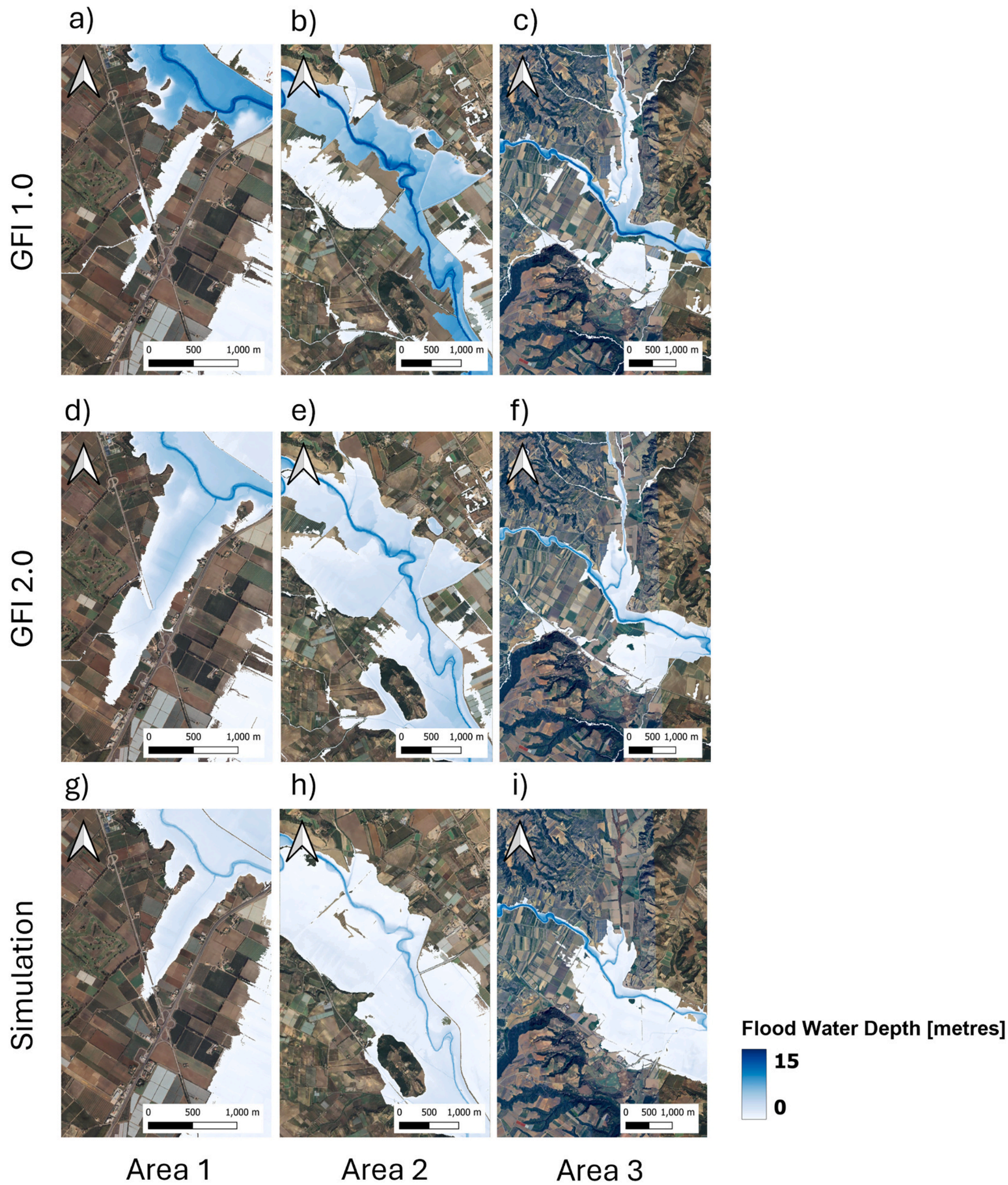

Fig. 12. Flood water depth based on return period T = 200 years. a-c) GFI 1.0; d-f) GFI 2.0; g-i) Hydraulic simulation (The presentation was rescaled based on the maximum and minimum flood water levels obtained through hydraulic simulation to facilitate comparison).

Validation against ISPRA flood hazard maps across 12 Italian basins, together with the detailed comparison against two-dimensional hydraulic simulations in the Bradano basin, showed that GFI 2.0 systematically improves the delineation of flood-prone areas relative to GFI 1.0. The most relevant gains occur in low-gradient floodplains, wide valleys, and confluence-dominated sectors, where local drainage connectivity alone is insufficient to explain inundation patterns. Improvements in flood water-depth estimation were also obtained, especially for the larger return periods, although these estimates remain first-order approximations rather than dynamic hydraulic solutions.

The analysis also showed that the benefit of the revised formulation is context dependent and computationally affordable. In mountainous and strongly confined basins, where downstream backwater effects are limited, GFI 1.0 and GFI 2.0 tend to perform similarly. Conversely, the added value of GFI 2.0 becomes more evident when coarser DEMs are used, making the method particularly suitable for large-area applications based on globally available elevation datasets. The runtime benchmark on the North Po basin confirms this scalability: full execution required about 1 min at 90 m, 7.6 min at 30 m, and 62.9 min at 10 m, while the confluence-aware backwater step itself contributed less than 0.3% of the total runtime even in the highest-resolution case. Overall, GFI 2.0 represents a targeted but significant advance in DEM-based flood susceptibility mapping. It provides a practical tool for regional screening, early-warning support, and preliminary planning in data-scarce environments, while also offering a physically grounded layer for integration with remote sensing, hybrid hydrologic-hydraulic workflows, and machine-learning approaches. Future research should focus on validation against observed flood events, testing across a broader range of climatic and geomorphic settings, and the inclusion of additional controls such as land use, anthropogenic infrastructure, and coastal or pluvial interactions.

CRediT authorship contribution statement

Salvatore Manfreda: Writing – review & editing, Writing – original draft, Visualization, Supervision, Resources, Project administration, Investigation, Funding acquisition, Conceptualization. **Jorge Saavedra Navarro:** Writing – review & editing, Writing – original draft, Validation, Software, Methodology, Investigation, Formal analysis, Data curation. **Cinzia Albertini:** Writing – review & editing, Visualization, Investigation. **Ruodan Zhuang:** Writing – review & editing, Validation, Methodology, Formal analysis. **Felice Daniele Pacia:** Writing – review & editing, Visualization, Formal analysis, Data curation. **Sadashiv Chaturvedi:** Writing – review & editing, Visualization, Formal analysis, Data curation. **Caterina Samela:** Writing – review & editing, Visualization, Supervision.

Declaration of competing interest

The authors declare that they have no known competing financial interests or personal relationships that could have appeared to influence the work reported in this paper.

Acknowledgement

This study was carried out within the RETURN Extended Partnership funded by the European Union Next-Generation EU (National Recovery and Resilience Plan -NRRP, Mission 4, Component 2, Investment 1.3—D. D. 1243 2/8/2022, PE0000005), the ESA MOST Dragon VI programme (DTE-CLIMATE: Digital Twin Earth Approach for Monitoring and Modelling Climate Change in Water, Energy and Carbon Cycles in Eurasia), and the CHANCES project (An Integrated Modelling Approach for Mitigating Climate Change Effects through Enhanced Weathering in Southern Italy -CUP E53D23021850001), and PhD in Sustainable Development and Climate Change, University School for Advanced Studies IUSS Pavia, carried out at University of Naples Federico II, Cycle XL, NRRP - funded by the European Union grants Innovative doctorates that respond to the innovation needs of companies, Ministerial Decree No. 630 of April 24, 2024, DM630/2024 – M4C2 - Inv. 3.3. - Dottorati Innovativi, I.3.3; and PhD Programme in Sustainable Development and Climate Change University School for Advanced Studies IUSS Pavia, carried out at University of Naples Federico II – XXXIX Cycle – Funded by the European Union NextgenerationEU - PNRR. Type of scholarship: DM118/2023 - M4C1 – Inv. 4.1 - Pubblica Amministrazione I53C23000820001.

Data availability

The MATLAB code used to test and apply GFI 2.0 is openly available at https://doi.org/10.5281/zenodo.18903835.

References

Abusarif, A.R., Nugroho, E.O., Riawan, E., Ferdiansyah, A., Andrean, R., Farid, M., Wahid, A.N., Bintang, J.A., Ardi, R., Wahid, N.H., Sari, I.A., 2023. Modified geomorphic flood index (GFI) method on backwater problem in tidal tropical river for rapid flood assessment. IOP Conference Series: Earth Environ. Sci. 1266 (1), 012064. IOP Publishing.

Albano, R., Mancusi, L., Adamowski, J., Cantisani, A., Sole, A., 2019. A GIS tool for mapping dam-break flood hazards in Italy. ISPRS Int. J. Geo-Inf. 8 (6). https://doi.org/10.3390/ijgi8060250 (WOS:000475307000008).

Albertini, C., Miglino, D., Iacobellis, V., De Paola, F., Manfreda, S., 2022. Delineation of flood-prone areas in cliffed coastal regions through a procedure based on the geomorphic flood index. J. Flood Risk Management 15 (1), e12766.

Albertini, C., Gioia, A., Iacobellis, V., Petropoulos, G.P., Manfreda, S., 2024. Assessing multi-source random forest classification and robustness of predictor variables in flooded areas mapping. Remote Sens. Appl.: Soc. Environ. 35, 101239. https://doi.org/10.1016/j.rsase.2024.101239.

Annis, A., Nardi, F., Morrison, R.R., Castelli, F., 2019. Investigating hydrogeomorphic floodplain mapping performance with varying DTM resolution and stream order. Hydrol. Sci. J. 64 (5), 525–538. https://doi.org/10.1080/02626667.2019.1591623.

Arcorace, M., Libertino, A., Alfieri, L., Gabellani, S., Matanò, A., Masoero, A., Basso, V., Boni, G., 2024. REFLEX—A novel method for the rapid estimation of flood extent. J. Flood Risk Management. https://doi.org/10.1111/jfr3.13034.

Aristizabal, F., Salas, F., Petrochenkov, G., Grout, T., Avant, B., Bates, B., Spies, R., Chadwick, N., Wills, Z., Judge, J., 2023. Extending height above nearest drainage to model multiple fluvial sources in flood inundation mapping applications for the U.S. National Water Model. Water Resour. Res. 59 (5), e2022WR032039. https://doi.org/10.1029/2022WR032039.

Balestra, F., Del Vecchio, M., Pirone, D., Persiano, S., Manfreda, S., Revellino, P., 2022. Flood susceptibility mapping using a deep neural network model: the case study of southern Italy. Environ. Sci. Proceedings 21 (1), 36. https://doi.org/10.3390/environsciproc2022021036.

Bintang, J.A., 2024. Sensitivity analysis of the geomorphology flood index to extreme rainfall variability in Indonesia. Calamity: A J. Disaster Technol. Eng. 2 (1), 53–69.

Blöschl, G., 2022. Three hypotheses on changing river flood hazards. Hydrol. Earth Syst. Sci. 26 (19), 5015–5033.

Blöschl, G., Nester, T., Komma, J., Parajka, J., Perdigão, R.A.P., 2013. The June 2013 flood in the upper Danube Basin, and comparisons with the 2002, 1954 and 1899 floods. Hydrol. Earth Syst. Sci. 17 (12), 5197–5212. https://doi.org/10.5194/hess-17-5197-2013.

Cea, L., Costabile, P., 2022. Flood risk in urban areas: modelling, management and adaptation to climate change. A review. Hydrology 9 (3), 50. https://doi.org/10.3390/hydrology9030050.

De Almeida, G.A.M., Bates, P., 2013. Applicability of the local inertial approximation of the shallow water equations to flood modeling. Water Resour. Res. 49 (8), 4833–4844. https://doi.org/10.1002/wrcr.20366.

Degiorgis, M., Gnecco, G., Gorni, S., Roth, G., Sanguineti, M., Taramasso, A.C., 2012. Classifiers for the detection of flood-prone areas using remote sensed elevation data. J. Hydrol. 470–471, 302–315.

Deiana, C., Deidda, R., Viola, F., 2023. Geomorphic floodplain mapping in small Mediterranean catchments using LiDAR data. Adv. Water Resour. 178, 104493.

Faridani, F., Bakhtiari, S., Faridhosseini, A., Nikpour, M.R., Mirzakhani, F., 2020. Estimating flood characteristics using geomorphologic flood index with regards to rainfall intensity-duration-frequency-area curves and CADDIES-2D model in three Iranian basins. Sustainability 12 (18), 7371. https://doi.org/10.3390/su12187371.

Fawcett, T., 2006. An introduction to ROC analysis. Pattern Recognit. Lett. 27 (8), 861–874.

Ferdiansyah, A., Nugroho, E.O., Riawan, E., Abusarif, A.R., Irwansyah, E., 2024. Modified geomorphic flood index (GFI) using land use parameter and effective rainfall ratio at Cikapundung River. E3S Web Conferences 513, 01003. https://doi.org/10.1051/e3sconf/202451301003.

Fiorentino, M., 1985. La valutazione dei volumi di piena nelle reti di drenaggio urbano. L'Idrotecnica 3, 141–152.

Galderisi, A., Fiore, P., Ferlisi, S., Petti, L., Plaitano, F., D'Andria, E., Viccione, G., Manfreda, S., Sole, A., 2024. Methods and tools to analyse and mitigate the seismic and flood risks in inland areas: A case study in the Campania region (southern Italy). Buildings 14 (4), 1015.

Gebrehiwot, A., Hashemi-Beni, L., 2022. 3D inundation mapping: a comparison between deep learning image classification and geomorphic flood index approaches. Front. Remote Sensing 3, 868104.

Guse, B., Merz, B., Wietzke, L., Ullrich, S., Viglione, A., Vorogushyn, S., 2020. The role of flood wave superposition in the severity of large floods. Hydrol. Earth Syst. Sci. 24 (4), 1633–1648. https://doi.org/10.5194/hess-24-1633-2020.

Hamouda, M.A., Awadallah, A.G., Abdel-Maguid, R.H., 2024. Extension of the geomorphic flood index classifier to predict flood inundation maps for uncalibrated rainfall depths in arid regions. Nat. Hazards 120, 4633–4655. https://doi.org/10.1007/s11069-023-06393-0.

Hawker, L., Uhe, P., Paulo, L., Sosa, J., Savage, J., Sampson, C., Neal, J., 2022. A 30 m global map of elevation with forests and buildings removed. Environ Res. Lett. 17, 024016.

Hawker, L., Bates, P., Neal, J., Rougier, J., 2018. Perspectives on digital elevation model (DEM) simulation for flood modeling in the absence of a high-accuracy open access global DEM. Front. Earth Sci. 6, 233.

Hawker, L., Neal, J., Savage, J., Kirkpatrick, T., Lord, R., Zylberberg, Y., Groeger, A., Thuy, T., Fox, S., Agyemang, F., Nam, P., 2024. Assessing LISFLOOD-FP with the next-generation digital elevation model FABDEM using household survey and remote sensing data in the central highlands of Vietnam. Nat. Hazards Earth Syst. Sci. 24 (2), 539–566 (WOS:001190497200001). https://doi.org/10.5194/nhess-24-539-2024.

Hermon, D., Adura Tengku Hamzah, T.A., Febriandi, R., Ramadhan, R., Putra, A., Rahmi, L., Sihaini, E., Sari, N., 2024. Characteristics of community adaptive resilience in overcoming the hazards of flood disaster in Kampar Regency-Indonesia. GEOMATE Journal 27 (122), 71–78. https://geomatejournal.com/geomate/article/view/4646.

Horton, R.E., 1945. Erosional development of streams and their drainage basins; hydrophysical approach to quantitative morphology. Geol. Soc. Am. Bull. 56 (3), 275 doi:10.1130/0016-7606(1945)56%255B275:EDOSAT%255D2.0.CO;2.

Hunter, N.M., Bates, P.D., Horritt, M.S., Wilson, M.D., 2007. Simple spatially-distributed models for predicting flood inundation: A review. Geomorphology 90 (3–4), 208–225. https://doi.org/10.1016/j.geomorph.2006.10.021.

Lastoria, B., Bussettini, M., Mariani, S., Piva, F., Braca, G., 2021. Rapporto sulle condizioni di pericolosità da alluvione in Italia e indicatori di rischio associati, 353/21. Istituto Superiore per la Protezione e la Ricerca Ambientale, Rapporti, Roma.

Leopold, L.B., Maddock, T., 1953. The hydraulic geometry of stream channels and some physiographic implications, 252. US Government Printing Office.

Link, O., Brox-Escudero, L.M., González, J., Link, R., 2019. A paleo-hydro-geomorphological perspective on urban flood risk assessment. Hydrol. Process. 33 (23), 3058–3072. https://doi.org/10.1002/hyp.13590.

Magnini, A., Lombardi, M., Persiano, S., Tirri, A., Lo Conti, F., Castellarin, A., 2022. Machine-learning blends of geomorphic descriptors: value and limitations for flood hazard assessment across large floodplains. Nat. Hazards Earth Syst. Sci. 22, 1469–1486. https://doi.org/10.5194/nhess-22-1469-2022.

Manfreda, S., Samela, C., 2019. A digital elevation model based method for a rapid estimation of flood inundation depth. J. Flood Risk Management 12 (S1), e12541. https://doi.org/10.1111/jfr3.12541.

Manfreda, S., Di Leo, M., Sole, A., 2011. Detection of flood prone areas using digital elevation models. J. Hydrol. Eng. 16 (10), 781–790. https://doi.org/10.1061/(ASCE)HE.1943-5584.0000367.

Manfreda, S., Samela, C., Gioia, A., Consoli, G., Iacobellis, V., Giuzio, L., Cantisani, A., Sole, A., 2015. Flood-prone areas assessment using linear binary classifiers based on flood maps obtained from 1D and 2D hydraulic models. Nat. Hazards 79 (2), 735–754. https://doi.org/10.1007/s11069-015-1869-5.

Mishra, A., Mukherjee, S., Merz, B., Singh, V.P., Wright, D.B., Villarini, G., Paul, S., Kumar, D.N., Khedun, C.P., Niyogi, D., Schumann, G., Stedinger, J.R., 2022. An overview of flood concepts, challenges, and future directions. J. Hydrol. Eng. 27 (6), 03122001. https://doi.org/10.1061/(ASCE)HE.1943-5584.0002164.

Mohanty, M., Tripathi, V., 2024. Can catchment attributes coupled with an Ensemble of Machine Learning improve flood Hazard mapping over large data-scarce catchments? EGU General Assembly 2024, EGU24–E9063. https://doi.org/10.5194/egusphere-egu24-9063.

Nardi, F., Biscarini, C., Di Francesco, S., Manciola, P., Ubertini, L., 2013. Comparing a large-scale DEM-based floodplain delineation algorithm with standard flood maps: the Tiber river basin case study. Irrig. Drain. 62 (S2). https://doi.org/10.1002/ird.1818.

Nardi, F., et al., 2019. GFPLAIN250m, a global high-resolution dataset of earth's floodplains. Sci. Data. https://doi.org/10.1038/sdata.2018.309.

Navarro, J.S., Zhuang, R., Albertini, C., Manfreda, S., 2025. Mapping flood susceptibility using random Forest exploiting satellite observations and geomorphic features. Sci. Total Environ. 1002, 180592. https://doi.org/10.1016/j.scitotenv.2025.180592.

Nobre, A.D., Cuartas, L.A., Momo, M.R., Severo, D.L., Pinheiro, A., Nobre, C.A., 2016. HAND contour: a new proxy predictor of inundation extent. Hydrol. Process. 30 (2), 320–333. https://doi.org/10.1002/hyp.10581.

Nugroho, P.C., Sutjiningsih, D., Kurniawan, L., 2019. Flood hazard assessment based on analysis of geomorphic flood index and history of flood events (case study in Kemuning watershed, Sampang). IOP Conference Series: Earth Environ. Sci. 366 (1), 012033.

Pacia, F.D., Pizzolla, T., Berterame, D., Galante, G., Manfreda, S., 2023. Planning flood mitigation interventions on the BRADANO River. L'Acqua, Agosto 109–118.

Pavesi, L., et al., 2024. Flood risk assessment through large-scale modeling under uncertainty. Nat. Hazards Earth Syst. Sci. https://doi.org/10.5194/nhess-24-4507-2024.

Perrini, P., Iacobellis, V., Gioia, A., Cea, L., 2025. A tracer-aided 2D numerical framework to define fluvial and pluvial hazard mapping. J. Flood Risk Management 18 (1). https://doi.org/10.1111/jfr3.13039.

Pratiwi, A.P., Rohmat, F.I.W., Nugroho, E.O., Farid, M., Kusuma, M.S.B., 2024. Flood hazard comparison based on geomorphic flood index and hydraulic HEC-RAS (case study in Ciliwung watershed, Jakarta). IOP Conf. Ser.: Earth Environ. Sci 1314 (1), 012084.

Rossi, F., Villani, P., 1998. A project for regional analysis of floods in Italy. In: Andah, K. (Ed.), Managing Hydro-Geological Disasters in a Vulnerable Environment. CNR Pub., pp. 141–168

Salim, G., Yehezkiel, A., Suryana, K., Irwansyah, E., 2023. Flood Hazard modelling in Jakarta using geomorphic flood index. IEEE Int. Conference Aerospace Electronics Remote Sensing Technol. (ICARES) 2023, 1–7. https://doi.org/10.1109/ICARES60489.2023.10329889.

Samela, C., Manfreda, S., De Paola, F., Giugni, M., Sole, A., Fiorentino, M., 2016. DEM-based approaches for the delineation of flood-prone areas in an Ungauged Basin in Africa. J. Hydrologic Eng. 21 (2), 04015044. https://doi.org/10.1061/(ASCE)HE.1943-5584.0001272.

Samela, C., Troy, T.J., Manfreda, S., 2017a. Geomorphic classifiers for flood-prone areas delineation for data-scarce environments. Adv. Water Resour. 102, 13–28.

Samela, C., Troy, T.J., Manfreda, S., 2017b. Dataset of 100-year flood susceptibility maps for the continental U.S. derived with a geomorphic method. Data Brief 12, 203–207. https://doi.org/10.1016/j.dib.2017.03.044.

Samela, C., Albano, R., Sole, A., Manfreda, S., 2018. A GIS tool for cost-effective delineation of flood-prone areas. Comput. Environ. Urban. Syst. 70, 43–52.

Samela, C., Carisi, F., Domeneghetti, A., Manfreda, S., 2023. A methodological framework for flood hazard assessment for land transport infrastructures. Int. J. Disaster Risk Reduction 85, 103491. https://doi.org/10.1016/j.ijdrr.2022.103491.

Sofia, G., Nikolopoulos, E.I., 2020. Floods and rivers: a circular causality perspective. Sci. Rep. 10 (1), 1–17. https://doi.org/10.1038/s41598-020-61533-x.

Strahler, A.N., 1952. Hypsometric (area-altitude) analysis of erosional topography. Geol. Soc. Am. Bull. 63 (11), 1117. https://doi.org/10.1029/TR038i006p00913.

Strahler, A.N., 1957. Quantitative analysis of watershed geomorphology. *Eos*. Trans. American Geophys. Union 38 (6), 913–920.

Talampas, W.D., Tarepe, D.A., 2019. Delineation of flood-prone areas in data-scarce environment using linear binary classifiers. Mindanao J. Sci. Technol. 17.

Tarquini, S., Isola, I., Favalli, M., Mazzarini, F., Bisson, M., Pareschi, M.T., Boschi, E., 2007. TINITALY/01: a new triangular irregular network of Italy. Ann. Geophys. https://doi.org/10.4401/ag-4424.

Tarquini, S., Isola, I., Favalli, M., Battistini, A., Dotta, G., 2023. TINITALY, a digital elevation model of Italy with a 10 meters cell size (Version 1.1). Istituto Nazionale di Geofisica e Vulcanologia (INGV). https://doi.org/10.13127/tinitaly/1.1.

Tavares da Costa, R., Manfreda, S., Luzzi, V., Samela, C., Mazzoli, P., Castellarin, A., Bagli, S., 2019. A web application for hydrogeomorphic flood hazard mapping. Environ. Model. Software 118, 172–186. https://doi.org/10.1016/j.envsoft.2019.04.010.

Tripathi, V., Mohanty, M.P., 2024. Can geomorphic flood descriptors coupled with machine learning models enhance in quantifying flood risks over data-scarce catchments? Development of a hybrid framework for Ganga basin (India). Environ. Sci. Pollut. Res. https://doi.org/10.1007/s11356-024-33507-3.

Virtriana, R., Retnowati, D.A., Rohayani, P., Sari, N.D., 2023. Comparative analysis of the MCDA and GFI methods in determining flood-prone areas in Jatinangor District, Sumedang. In: The International archives of the photogrammetry, remote sensing and spatial information Sciences, XLVIII-M-3-2023, pp. 261–266. https://doi.org/10.5194/isprs-archives-XLVIII-M-3-2023-261-2023.

Wagner, W., et al., 2026. The fullyautomatic Sentinel1 global flood monitoring service. Remote Sens. Environ. https://doi.org/10.1016/j.rse.2025.115108.

Wing, O.E.J., Bates, P.D., Quinn, N.D., Savage, J.T.S., Uhe, P.F., Cooper, A., Collings, T. P., Addor, N., Lord, N.S., Hatchard, S., Hoch, J.M., Bates, J., Probyn, I., Himsworth, S., Rodríguez González, J., Brine, M.P., Wilkinson, H., Sampson, C.C., Smith, A.M., Haigh, I.D., 2024. A 30 m global flood inundation model for any climate scenario. Water Resour. Res. 60 (8), e2023WR036460. https://doi.org/10.1029/2023WR036460.

Winsemius, H.C., Aerts, J.C.J.H., Van Beek, L.P.H., Bierkens, M.F.P., Bouwman, A., Jongman, B., Kwadijk, J.C.J., Ligtvoet, W., Lucas, P.L., Van Vuuren, D.P., 2016. Global drivers of future river flood risk. Nat. Clim. Chang. 6 (4), 381–385.

Yamazaki, D., Ikeshima, D., Tawatari, R., Yamaguchi, T., O'Loughlin, F., Neal, J.C., Sampson, C.C., Kanae, S., Bates, P.D., 2017. A high accuracy map of global terrain elevations. Geophys. Res. Lett. 44, 5844–5853. https://doi.org/10.1002/2017GL072874.

Yan, G., Yuan, S., Tang, H., Xu, D., Liu, M., Whittaker, C., Gualtieri, C., 2024. Hydrodynamic response of channel flow confluence to the tributary floodplain topography. Water Resour. Res. 60 (8), e2023WR036244. https://doi.org/10.1029/2023WR036244.

Yolina, H., Rojali, Irwansyah, E., 2023. Development of flood-prone area classification program using linear classifier method based on geomorphic flood index and land cover. Procedia Comput. Sci. 216, 396–405. https://doi.org/10.1016/j.procs.2022.12.151.

Zheng, K., et al., 2024. SHIFT: a spatial-heterogeneity improvement in DEM-based mapping of global geomorphic floodplains. Earth System Sci. Data. https://doi.org/10.5281/zenodo.11835133.